The finite element method and convergence theory for the EEG forward problem solution

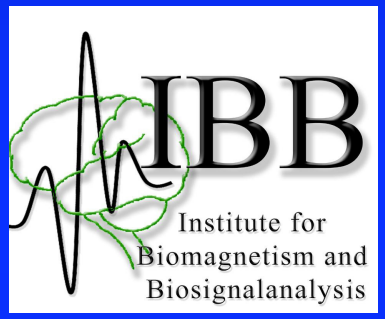

Carsten H. Wolters

Institut für Biomagnetismus und Biosignalanalyse, Westf. Wilhelms-Universität Münster, Germany

Lectures on Nov.12, 2024

Structure of the lecture

- Convergence analysis for FEM subtraction approach (sections 6.5.1-6.5.3 of lecture scriptum)
- Other source models (section 6.5.4 of lecture scriptum)
- Overview: Multi-layer sphere model (section 6.2 of lecture scriptum)
- Forward modeling results
- The local subtraction approach

[Wolters et al., *SIAM J Sci Comp*, 2007]
[Drechsler et al., *NeuroImage*, 2009]
[Wolters, *Lecture scriptum*]

Overview: Subtraction approach

$$\nabla \cdot (\sigma \nabla \Phi) = \nabla \cdot \mathrm{j}^p = \mathrm{J}^p \ \text{ in } \Omega, \tag{6.1}$$

$$\langle \sigma \nabla \Phi, \mathrm{n} \rangle|_\Gamma = 0, \tag{6.2}$$

$$\Phi(x_{\mathrm{ref}}) = 0\,. \tag{6.3}$$

$$\mathrm{J}^p(x) = \nabla \cdot \mathrm{j}^p(x) := \nabla \cdot \mathrm{M}\delta(x - x_0)\,. \tag{6.4}$$

$$-\nabla \cdot (\sigma \nabla \Phi^{\mathrm{corr}}) = f \ \text{ in } \Omega, \qquad f := \nabla \cdot (\sigma^{\mathrm{corr}} \nabla \Phi^{\infty}), \tag{6.11}$$

mit inhomogenen Neumann Randbedingungen an der Kopfoberfläche

$$\langle \sigma \nabla \Phi^{\mathrm{corr}}, \mathrm{n} \rangle = g \ \text{ on } \Gamma, \qquad g := -\langle \sigma \nabla \Phi^{\infty}, \mathrm{n} \rangle. \tag{6.12}$$

[Wolters et al., *SIAM J Sci Comp*, 2007]
[Drechsler et al., *NeuroImage*, 2009]
[Wolters, *Lecture scriptum*]

Subtraction finite element approach

Theorem 6.1.37 (Existenz und Eindeutigkeit). *Sei Ω kompakt mit stückweise glattem Rand und erfülle eine Kegelbedingung. Dann hat die Variationsaufgabe*

$$\text{Suche } v \in H^1_*(\Omega): \quad J(v) := \frac{1}{2}a(v,v) - l(v) \to min! \tag{6.38}$$

mit $a(\cdot,\cdot)$ aus (6.34) und $l(\cdot)$ aus (6.35) genau eine Lösung $\Phi^{corr} \in H^1_*(\Omega)$. Diese Lösung ist durch

$$a(\Phi^{corr}, v) = l(v) \quad \forall v \in H^1(\Omega) \tag{6.39}$$

charakterisiert.

$$a(\Phi^{\text{corr}}, v) := \int_\Omega \langle \sigma \nabla \Phi^{\text{corr}}, \nabla v \rangle d\Omega \tag{6.34}$$

$$l(v) := \int_\Omega f v d\Omega + \int_\Gamma g v d\Gamma \tag{6.35}$$

Because of the smoothness of the functions in equations (6.11) and (6.12), we could apply the Gauß integral theorem

$$\int_\Omega v(x)\text{div}\sigma(x)\nabla u(x)dx = -\int_\Omega \langle \nabla v(x), \sigma(x)\nabla u(x)\rangle dx + \int_\Gamma v(x)\langle n(x), \sigma(x)\nabla u(x)\rangle dx$$

and in Theorem 6.1.37 we arrived at the variational formulation that was suitable for a finite element discretisation. Here, we rewrite it in a slightly different form. We now indicate the source position by an index y. For example, $\sigma(y)$ is now the conductivity at the source position which was denoted by σ^∞ in equation 6.9.

[Wolters et al., *SIAM J Sci Comp*, 2007]
[Drechsler et al., *NeuroImage*, 2009]
[Wolters, *Lecture scriptum*]

Subtraction finite element approach

This leads to

Definition 6.5.1 (Analytical forward problem). *For an arbitrary mapping* $\alpha : \Omega \to \mathbb{R}^{3\times 3}$ *we define the bilinear form*

$$a_\alpha : V \times V \to \mathbb{R}, \quad a_\alpha(u,v) := \int_\Omega \langle \alpha(x)\nabla u(x), \nabla v(x)\rangle dx.$$

The weak formulation of the analytical forward problem (Equations (6.11) and (6.12)) was to find $\Phi^{corr} \in V$ *s.t. for all* $v \in V$

$$\begin{aligned} a_\sigma(\Phi^{corr,y}, v) &= a_{\sigma(y)-\sigma}(\Phi^{\infty,y}, v) - \int_{\partial\Omega} v(x)\langle n(x), \sigma(y)\nabla\Phi^{\infty,y}(x)\rangle dx, \\ \int_\Omega \Phi^{corr,y}(x)dx &= -\int_\Omega \Phi^{\infty,y}(x)dx. \end{aligned}$$

In Theorem 6.1.37, it was shown that a unique solution of the analytical forward problem exists and the solution $\Phi^{corr,y}$ belongs to $H^1(\Omega)$.

[Braess, Finite Elemente, 2007]

FEM basis functions and meshing aspects

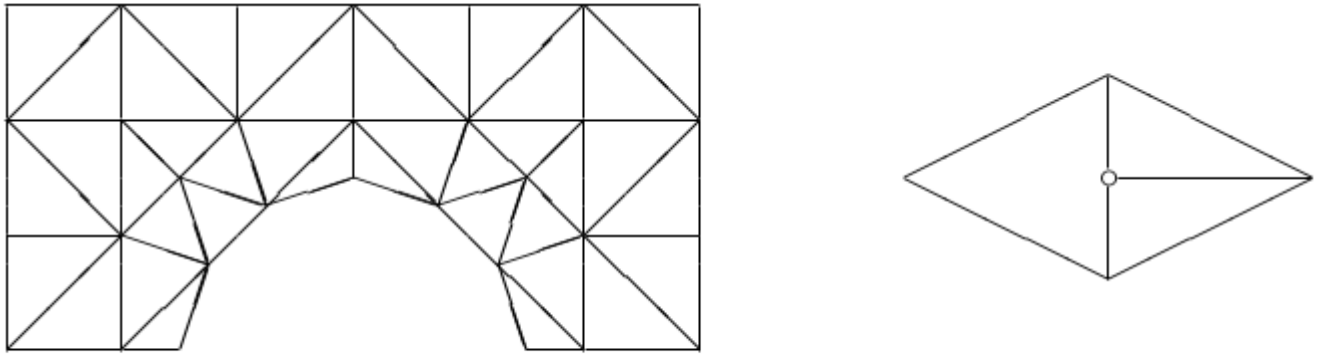

Abb. 12. Erlaubte Triangulierung und unzulässige Triangulierung mit hängendem Knoten

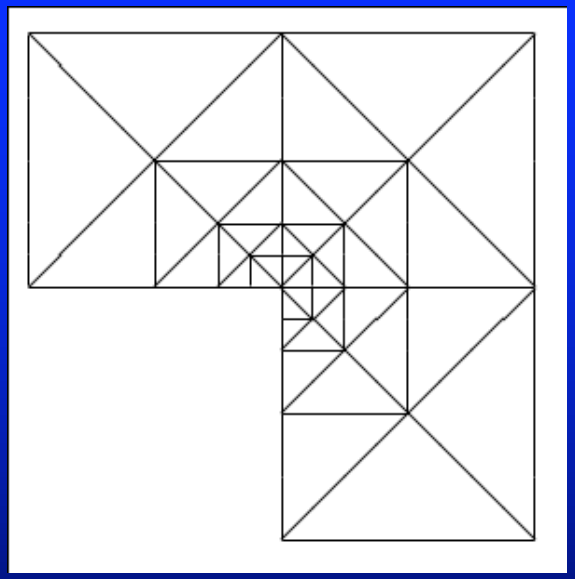

[Braess, Finite Elemente, 2007]

FEM basis functions and meshing aspects

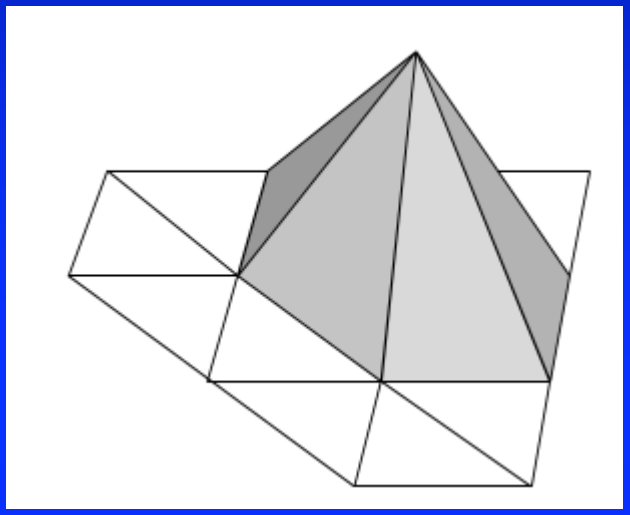

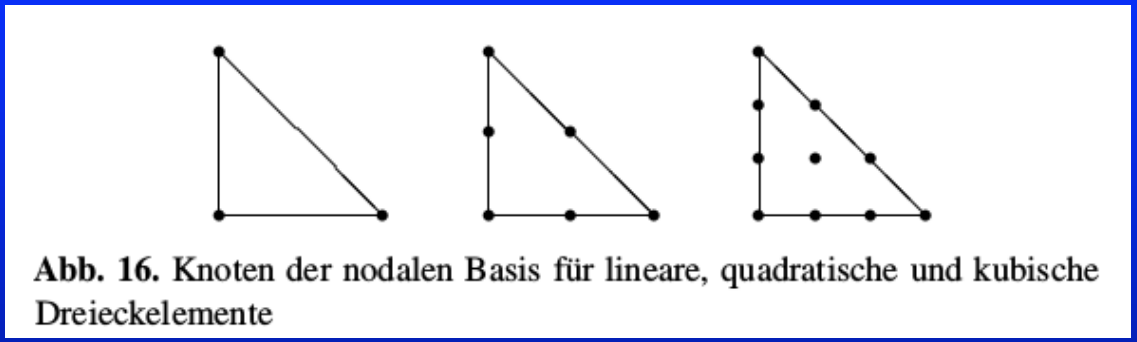

Abb. 16. Knoten der nodalen Basis für lineare, quadratische und kubische Dreieckelemente

Tabelle 2. Interpolation bei gebräuchlichen Finiten Elementen

- Vorgabe des Funktionswertes
- Vorgabe von Funktionswert und den 1. Ableitungen
- Vorgabe von Funktionswert, 1. und 2. Ableitungen
- Vorgabe der Normalableitung

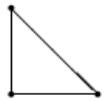	Lineares Dreieckelement $\mathcal{M}_0^1$ $u \in C^0(\Omega)$ $\Pi_{\text{ref}} = \mathcal{P}_1, \quad \dim \Pi_{\text{ref}} = 3$
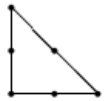	Quadratisches Dreieckelement $\mathcal{M}_0^2$ $u \in C^0(\Omega)$ $\Pi_{\text{ref}} = \mathcal{P}_2, \quad \dim \Pi_{\text{ref}} = 6$
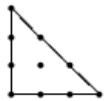	Kubisches Dreieckelement $\mathcal{M}_0^3$ $u \in C^0(\Omega)$ $\Pi_{\text{ref}} = \mathcal{P}_3, \quad \dim \Pi_{\text{ref}} = 10$
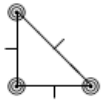	Argyris Dreieck $u \in C^1(\Omega)$ $\Pi_{\text{ref}} = \mathcal{P}_5, \quad \dim \Pi_{\text{ref}} = 21$
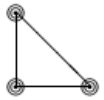	Bell Dreieck $u \in C^1(\Omega)$ $\Pi_{\text{ref}} \subset \mathcal{P}_5, \ \partial_\nu u\|_{\partial T_i} \in \mathcal{P}_3, \quad \dim \Pi_{\text{ref}} = 18$
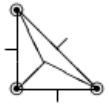	Hsieh–Clough–Tocher–Element $u \in C^1(\Omega)$ $T = \bigcup_{i=1}^3 K_i, \quad u\|_{K_i} \in \mathcal{P}_3, \quad \dim \Pi_{\text{ref}} = 12$
	Bilineares Viereckelement Q_1 $u \in C^0(\Omega)$ $\Pi_{\text{ref}} \subset \mathcal{P}_2, \ u\|_{\partial T_i} \in \mathcal{P}_1, \quad \dim \Pi_{\text{ref}} = 4$
	Viereckelement der Serendipity-Klasse $u \in C^0(\Omega)$ $\Pi_{\text{ref}} \subset \mathcal{P}_3, \ u\|_{\partial T_i} \in \mathcal{P}_2, \quad \dim \Pi_{\text{ref}} = 8$

[Wolters et al., *SIAM J Sci Comp*, 2007]
[Drechsler et al., *NeuroImage*, 2009]
[Wolters, *Lecture scriptum*]

FEM basis functions and meshing aspects

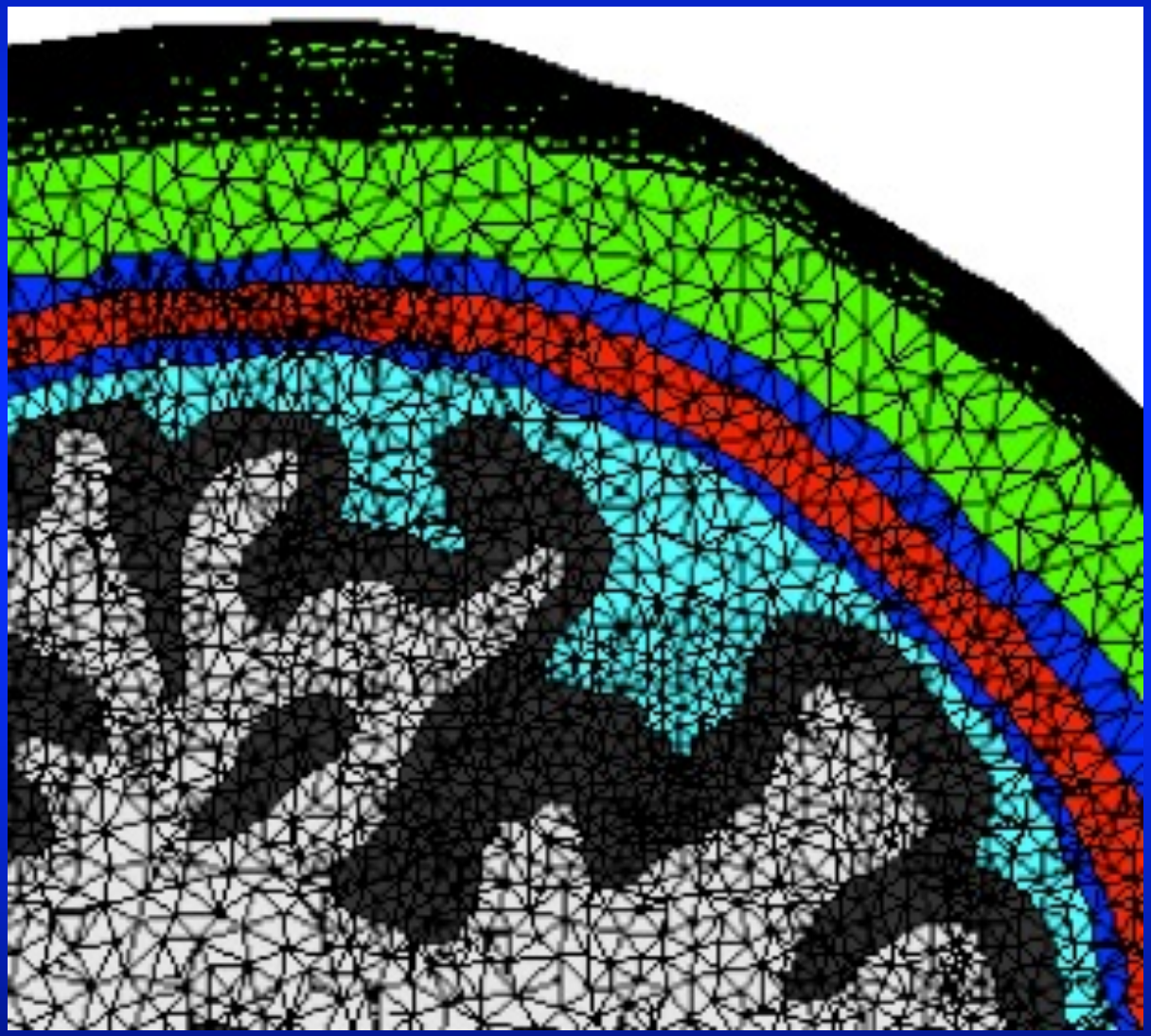

Subtraction FEM approach

[Wolters et al., *SIAM J Sci Comp*, 2007]
[Drechsler et al., *NeuroImage*, 2009]
[Wolters, *Lecture scriptum*]

Let $\tau = \{\tau_1, \ldots, \tau_T\}$ be a triangulation of the polygonal domain Ω into tetrahedra τ_i. For the finite element space V_N we use standard conforming linear elements, i.e. $V_N = \{v \in V \mid v|_{\tau_i} \text{ affine }, i = 1, \ldots, T\}$. Let $\text{span}\{\varphi_i \mid i \in I\}$ denote the standard Lagrange basis of V_N using local basis functions φ_i, $i \in I, \#I = N$. By ξ_i we denote the Lagrange point of the FE basis function φ_i.

Definition 6.5.2 (Finite element forward problem)**.** *The finite element forward problem is to find $u_N \in V_N$ s.t. for all $v \in V_N$*

$$
\begin{aligned}
a_\sigma(u_N, v) &= a_{\sigma(y)-\sigma}(\Phi^{\infty,y}, v) - \int_\Gamma v(x)\langle n(x), \sigma(y)\nabla\Phi^{\infty,y}(x)\rangle dx, \\
\int_\Omega u_N(x)dx &= -\int_\Omega \Phi^{\infty,y}(x)dx.
\end{aligned}
$$

$$u_N = \sum_i u^{[i]} \varphi_i$$

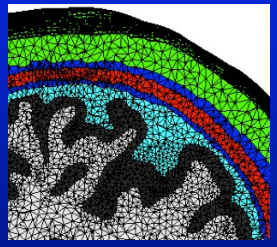

Subtraction FEM approach

[Wolters et al., *SIAM J Sci Comp*, 2007]
[Drechsler et al., *NeuroImage*, 2009]
[Wolters, *Lecture scriptum*]

Numerics of the full subtraction approach

The finite element approach leads to the following linear system for the *full subtraction approach*:

$$Ku = b^y, \quad K \in \mathbb{R}^{N\times N},\ u, b^y \in \mathbb{R}^N \tag{6.110}$$

with the stiffness matrix

$$K_{i,j} := \int_\Omega \langle \sigma(x)\nabla\varphi_j, \nabla\varphi_i\rangle dx, \quad i,j = 1,\ldots,N \tag{6.111}$$

and the right-hand side

$$b_i^y := \int_\Omega \langle (\sigma(y)-\sigma(x))\nabla\Phi^{\infty,y}(x), \nabla\varphi_i(x)\rangle dx \tag{6.112}$$

$$- \int_\Gamma \varphi_i(x)\langle n(x), \sigma(y)\nabla\Phi^{\infty,y}(x)\rangle dx, \quad i = 1,\ldots,N. \tag{6.113}$$

Subtraction FEM approach

[Wolters et al., *SIAM J Sci Comp*, 2007]
[Drechsler et al., *NeuroImage*, 2009]
[Wolters, *Lecture scriptum*]

The matrix K is SPD, where the positive definiteness follows from the ellipticity of the bilinear form $a(\cdot,\cdot)$ for all $u_N \in \mathbb{V}_N$,

$$u^{tr} K u = \sum_{i,j} u^{[j]} K^{[ij]} u^{[i]} = a\left(\sum_j u^{[j]} \varphi_j, \sum_i u^{[i]} \varphi_i\right) = a(u_N, u_N) \overset{\text{Lemma } 6.1.34}{\geq} C_{\text{ell}} \|u_N\|_1^2, \tag{6.114}$$

with $C_{\text{ell}} > 0$ the ellipticity constant and from the comments of Schwarz [282, Chapter 3.1.3] concerning the implementation of the Dirichlet condition.

Full subtraction approach

[Wolters et al., *SIAM J Sci Comp*, 2007]
[Drechsler et al., *NeuroImage*, 2009]
[Wolters, *Lecture scriptum*]

The term $\nabla\varphi_i$ is constant for linear elements, so that entries of K in (6.111) can be computed easily. The entries of the right-hand side b^y need to be accurate enough in order to preserve the finite element convergence. The gradient of $\Phi^{\infty,y}$ can be computed analytically following equation (6.10). Since we project the

correction potential into the space of piecewise linear elements, it is sufficient to have a perturbation of an order of the square of the step size which is achieved by a second order accurate quadrature formula. In Section 6.5.9 we will verify that this order is necessary and sufficient to produce a negligible quadrature error. We assemble the first term (6.112) of b_i^y element-wise. For $x \to y$, the integral even vanishes because of the homogeneity assumption. The second term (6.113) involves the normal vector and the basis function itself. Thus, we need a quadrature formula that resolves $\nabla\Phi^{\infty,y}$ at the boundary (where it is very smooth) and that is accurate for linear functions. Again, a second order quadrature formula for the surface triangles is necessary and sufficient, as will be verified in Section 6.5.9.

Full subtraction approach

[Wolters et al., *SIAM J Sci Comp*, 2007]
[Drechsler et al., *NeuroImage*, 2009]
[Wolters, *Lecture scriptum*]

Table 6.1: Quadrature formulas of Stroud [307] for the volume integral from Equation (6.112) and the surface integral from Equation (6.113) .

Formula	degree	number integration points	Reference
Volume integral from Equation (6.112)			
$T_n : 1-1$	1	1	[307, Chapter 8.8, p.307]
$T_n : 2-1$	2	$n+1$	[307, Chapter 8.8, p.307]
$T_3 : 7-1$	7	64	[307, Chapter 8.8, p.315]
Surface integral from Equation (6.113)			
$T_n : 1-1$	1	1	[307, Chapter 8.8, p.307]
$T_n : 2-1$	2	$n+1$	[307, Chapter 8.8, p.307]
$T_2 : 7-1$	7	16	[307, Chapter 8.8, p.314]

For the numerical integration of the right-hand side (6.112), (6.113), we use quadrature formulas of [307]. As shown in Table 6.1, the overall numerical accuracy of the full subtraction approach will be evaluated for quadrature orders of 1, 2 and 7. Our notation in Table 6.1 closely follows the one of the tables in [307]. T_n indicates an n-dimensional simplex [307, Chapter 7.8] (in our case: $n = 3$).

Projected (or approx.) subtraction source modeling approach

Projected subtraction FEM

[Wolters et al., *SIAM J Sci Comp*, 2007]
[Drechsler et al., *NeuroImage*, 2009]
[Wolters, *Lecture scriptum*]

Numerics of the projected subtraction approach

In [370], a *projected subtraction approach* was presented where the function $\Phi^{\infty,y}$ is projected in the finite element space by

$$\Phi^{\infty}(x) \approx \Phi_N^{\infty}(x) = \sum_{j=1}^{N} \varphi_j(x)\Phi_j^{\infty}, \quad \Phi_j^{\infty} = \Phi^{\infty}(\xi_j). \tag{6.115}$$

Introducing the coefficient vector $\Phi_{\infty} := (\Phi_1^{\infty}, \ldots, \Phi_N^{\infty})$, the system of equations

$$Ku = -K^{corr}\Phi_{\infty} - S\Phi_{\infty} \tag{6.116}$$

was obtained where K was defined in (6.111) and the matrices K^{corr} and S are defined by

$$K_{i,j}^{corr} := -\int_{\Omega} \langle (\sigma(y) - \sigma(x))\nabla\varphi_j(x), \nabla\varphi_i(x)\rangle dx \tag{6.117}$$

and

$$S_{i,j} := \int_{\partial\Omega} \langle \sigma(y)\nabla\varphi_j(x), n(x)\rangle \varphi_i(x) dx. \tag{6.118}$$

Projected subtraction FEM

[Wolters et al., *SIAM J Sci Comp*, 2007]
[Drechsler et al., *NeuroImage*, 2009]
[Wolters, *Lecture scriptum*]

Even if the projected subtraction approach is computationally less expensive because for each source, only the coefficient vector u_∞ has to be computed, the drawback of the approach is the additional approximation error by (6.115). We will see in the numerical validation section that the presented full subtraction approach in which Φ^∞ is not approximated in the FE space has a much higher degree of accuracy, but is, however, also significantly more expensive with regard to the computational amount of work.

Convergence analysis

[Wolters et al., *SIAM J Sci Comp*, 2007]
[Drechsler et al., *NeuroImage*, 2009]
[Wolters, *Lecture scriptum*]

6.5.2 Convergence analysis for the subtraction approach

In this section we will see that the L^2-error of the approximation

$$\varepsilon_N := \|\Phi_h^{\text{corr}} - \Phi^{\text{corr}}\|_{L^2(\Omega)}$$

with Φ_h^{corr} being the finite element approximation with FE stepsize h to the function Φ^{corr} behaves like $h^2 = N^{-2/3}$, so we have to use a finite dimensional but large space V_N. For our FE approximation Φ_h^{corr}, we are interested in estimates of the form

$$||\Phi^{corr} - \Phi_h^{corr}|| \leq Ch^k \tag{6.119}$$

with largest possible quantitative order k. h denotes the edge length of a finite element. In general, the order depends

- on the regularity of the solution
- on the degree of the FE trial-functions
- on the chosen Sobolev norm and
- on the approximation properties of the triangulation to the geometry.

Convergence analysis

[Wolters et al., *SIAM J Sci Comp*, 2007]
[Drechsler et al., *NeuroImage*, 2009]
[Wolters, *Lecture scriptum*]

For a **single compartment volume conductor model with homogeneous conductivity**, we have the following property:

Theorem 6.5.3 (Quantitative error estimate for single compartment model with homogeneous conductivity [121]). *Let us assume a sufficiently regular solution* $\Phi^{corr} \in H^2(\Omega)$. *For an appropriate tetrahedralization (hexahedralization), linear (trilinear) FE trial-functions and a continuous and elliptic bilinear form* $a(\cdot,\cdot)$, *we find a constant* C_1 *which is independent of* Φ^{corr} *and* h *with*

$$||\Phi^{corr} - \Phi_h^{corr}||_1 \leq C_1 h ||\Phi^{corr}||_2.$$

In the single compartment volume conductor model with homogeneous conductivity, the regularity assumption $\Phi^{corr} \in H^2(\Omega)$ is typically fulfilled because the boundary of the domain Ω is piecewise smooth.

Convergence analysis

[Wolters et al., *SIAM J Sci Comp*, 2007]
[Drechsler et al., *NeuroImage*, 2009]
[Wolters, *Lecture scriptum*]

Lemma 6.5.4 (Aubin-Nitsche [121]). *Let us assume a sufficiently regular solution* $\Phi^{corr} \in H^2(\Omega)$. *For an appropriate tetrahedralization (hexahedralization), linear (trilinear) FE trial-functions and a continuous and elliptic bilinear form* $a(\cdot,\cdot)$, *we find a constant* C_2 *which is independent of* Φ^{corr} *and* h *with*

$$||\Phi^{corr} - \Phi_h^{corr}||_0 \leq C_2 h^2 ||\Phi^{corr}||_2.$$

Convergence analysis

[Wolters et al., *SIAM J Sci Comp*, 2007]
[Drechsler et al., *NeuroImage*, 2009]
[Wolters, *Lecture scriptum*]

For a **multi-layer model with discontinuous conductivities**, we can only assume $\Phi^{corr} \in H^1(\Omega)$ (as discussed above, due to higher regularity assumptions, it might be $\Phi^{corr} \in H^{1+\varepsilon}(\Omega)$). Following Hackbusch [121] (Chapter 10.1.2), we can hope that the general error bounds $||\Phi^{corr} - \Phi_h^{corr}||_1 = O(h)$ and $||\Phi^{corr} - \Phi_h^{corr}||_0 = O(h^2)$ can be achieved by means of isoparametric, i.e., geometry conforming, finite elements.

With regard to our specific application, we can give a statement concerning the property of the constant C in Equation (6.119), which will be of practical interest, as shown later in the simulation studies.

Convergence analysis

[Wolters et al., *SIAM J Sci Comp*, 2007]
[Drechsler et al., *NeuroImage*, 2009]
[Wolters, *Lecture scriptum*]

Lemma 6.5.5. *Let δ be the distance between the source position x_0 and the closest location of the next conductivity jump on $\partial\Omega^{\infty}$ (see definitions in Section 6.1.2). If δ gets small, then the constant $C(\delta)$ in*

$$|l(v)| \leq C(\delta)||v||_{L_2(\Omega)}, \quad \forall v \in H^1(\Omega),$$

with $l(v)$ from Equation (6.35) is proportional to $\delta^{-5/2}$ ($c_1(\delta) \approx \delta^{-5/2}$).

Convergence analysis

[Wolters et al., *SIAM J Sci Comp*, 2007]
[Drechsler et al., *NeuroImage*, 2009]
[Wolters, *Lecture scriptum*, 2016]

Proof. When defining $r := x - x_0$, we find $|\Delta\Phi^\infty| \approx 1/|r|^4$ and, with $\bar{\Omega} := \Omega \setminus \Omega^\infty$,

$$||\Delta\Phi^\infty||_{L_2(\bar{\Omega})} = \sqrt{\int_{\bar{\Omega}} (\Delta\Phi^\infty)^2 \, dx} \approx \sqrt{\int_{|r|\geq\delta} 1/r^8 dr} \approx \sqrt{1/\delta^5} = \delta^{-5/2} =: c_1(\delta).$$

We then find constants $C(\delta)$ and c_2, so that

$$\begin{aligned}
|l(v)| &\overset{(6.35)}{=} \left| \int_\Omega \nabla \cdot (\sigma^{\text{corr}} \nabla\Phi^\infty) \, v dx - \int_\Gamma \langle \sigma \nabla\Phi^\infty, \mathbf{n} \rangle v d\Gamma \right| \\
&\leq \int_\Omega |\nabla \cdot (\sigma^{\text{corr}} \nabla\Phi^\infty) \, v| \, dx + c_2 ||v||_{L_2(\Omega)} \\
&\leq \sigma^{\text{corr}}_{\max} \int_{\bar{\Omega}} ||\Delta\Phi^\infty|| \, ||v|| dx + c_2 ||v||_{L_2(\Omega)} \\
&\overset{\text{Hölder}}{\leq} \sigma^{\text{corr}}_{\max} ||\Delta\Phi^\infty||_{L_2(\bar{\Omega})} ||v||_{L_2(\bar{\Omega})} + c_2 ||v||_{L_2(\Omega)} \\
&\leq (\sigma^{\text{corr}}_{\max} c_1(\delta) + c_2) \, ||v||_{L_2(\Omega)} \leq C(\delta) ||v||_{L_2(\Omega)}
\end{aligned}$$

□

Convergence analysis

[Wolters et al., *SIAM J Sci Comp*, 2007]
[Drechsler et al., *NeuroImage*, 2009]
[Wolters, *Lecture scriptum*]

Lemma 6.5.5 has to be interpreted in the following way. If the source approaches a next conductivity jump, i.e., if δ goes to 0, then the constant for the upper estimation of the right-hand side functional l gets larger (with exponent $5/2$).

Convergence analysis

[Wolters et al., *SIAM J Sci Comp*, 2007]
[Drechsler et al., *NeuroImage*, 2009]
[Wolters, *Lecture scriptum*]

Lemma 6.5.6. *With l from Equation (6.35), we find*

$$||\Phi^{corr}||_0 \leq C_{\text{ell}}^{-1}||l||_0$$

Proof. The ellipticity of the bilinear form was used:

$$C_{\text{ell}}||\Phi^{corr}||_0^2 \leq C_{\text{ell}}||\Phi^{corr}||_1^2 \overset{\text{Lemma 6.1.34}}{\leq} a(\Phi^{corr}, \Phi^{corr}) = (l, \Phi^{corr}) \leq ||l||_0||\Phi^{corr}||_0.$$

□

Convergence analysis

[Wolters et al., *SIAM J Sci Comp*, 2007]
[Drechsler et al., *NeuroImage*, 2009]
[Wolters, *Lecture scriptum*]

In summary, we thus find

$$||\Phi^{corr} - \Phi_h^{corr}||_0 \overset{Lemma\ 6.5.4}{\leq} C_2\, ||\Phi^{corr}||_2\, h^2 \overset{Lemma\ 6.5.6}{\leq} C_3\, ||l||_0\, h^2 \overset{Lemma\ 6.5.5}{\leq} C(\delta)\, C_3\, h^2.$$

For sources close to the next conductivity jump (e.g., sources with high eccentricity, see numerical studies in Section 6.5.8), we have to be aware of possibly larger numerical errors because of a strongly increasing constant $C(\delta)$.

Structure of the lecture

- Convergence analysis for FEM subtraction approach (sections 6.5.1-6.5.3 of lecture scriptum)
- Other source models (section 6.5.4 of lecture scriptum)
- Overview: Multi-layer sphere model (section 6.2 of lecture scriptum)
- Forward modeling results
- The local subtraction approach

Source models

[Wolters, *Lecture scriptum*]

The *subtraction method* was presented above as one way to address the source singularity. The subtraction FE approach was shown to have a sound mathematical basis for point current dipole models. Another family of source representation methods, known as *direct FE approaches* to the total potential [388; 10; 41; 355;

271; 178], are computationally less expensive, but also mathematically less sound under the assumption that a point dipole is the more realistic source model. However, if the realistic extent of an activated patch of cortical neurons is taken into account, a smoother source model might even be more appropriate.

Partial integration (PI) source modeling approach

Partial integration (PI)

[Wolters, *Lecture scriptum*]

The first direct method, discussed in the following, is the so-called *partial integration direct FE approach*. Multiplying both sides of Equation (6.1) by a linear FE basis function φ_i and integrating over the head domain leads to a partial integration direct approach for the total potential [10; 355; 206] expressed as

$$\int_\Omega \nabla \cdot (\sigma \nabla \Phi)\, \varphi_i dx = \int_\Omega \nabla \cdot \mathbf{j}^p \varphi_i dx.$$

Integration by parts, applied to both sides of the above equation, yields

$$-\int_\Omega \langle \sigma \nabla \Phi, \nabla \varphi_i \rangle dx + \int_\Gamma \langle \sigma \nabla \Phi, \mathbf{n} \rangle \varphi_i d\Gamma = -\int_\Omega \langle \mathbf{j}^p, \nabla \varphi_i \rangle dx + \int_\Gamma \langle \mathbf{j}^p, \mathbf{n} \rangle \varphi_i d\Gamma.$$

Partial integration (PI)

[Wolters, *Lecture scriptum*]

Using the homogeneous Neumann boundary condition from Equation (6.2) and the fact that the current density vanishes on the head surface, we arrive at

$$\int_\Omega \langle \sigma \nabla \Phi, \nabla \varphi_i \rangle dx = \int_\Omega \langle \mathbf{j}^p, \nabla \varphi_i \rangle dx \overset{(6.4)}{=} \langle \mathbf{M}_0, \nabla \varphi_i(\mathbf{x}_0) \rangle.$$

Setting $\Phi(\mathbf{x}) \approx \Phi_h(\mathbf{x}) = \sum_{j=1}^{N_h} \varphi_j(\mathbf{x}) \underline{u}_h^{[j]}$, leads to the linear system

$$K_h \underline{u}_h = \underline{j}_{\mathrm{PI},h}, \tag{6.120}$$

with the same stiffness matrix as in (6.111) and the right-hand side vector $\underline{j}_{\mathrm{PI},h} \in \mathbb{R}^{N_h}$ with entries

$$\underline{j}_{\mathrm{PI},h}^{[i]} = \begin{cases} \langle \mathbf{M}_0, \nabla \varphi_i(\mathbf{x}_0) \rangle & \text{if } i \in \textsc{NodesOfEle}(\mathbf{x}_0), \\ 0 & \text{otherwise.} \end{cases} \tag{6.121}$$

The partial integration source model

[Wolters, *Lecture scriptum*]

The function NODESOFELE($\mathbf{x}_0$) determines the set of nodes of the element which contains the dipole at position $\mathbf{x}_0$. Note that while the right-hand side vectors of the full subtraction approach (see (6.112) and (6.113)) and of the projected subtraction approach (see Equation (6.116)) are fully populated, $\underline{j}_{\mathrm{PI},h}$ has only |NODESOFELE| non-zero entries. Here, $|\cdot|$ denotes the number of elements in the set NODESOFELE.

For the linear basis functions φ_i considered in the following, the right-hand side (6.121) and thus the computed solution for the total potential in (6.120) will be constant for all $\mathbf{x}_0$ within a finite element.

Right-hand side vector has only 4 (for tetrahedra models) non-zero entries and can be computed very fast

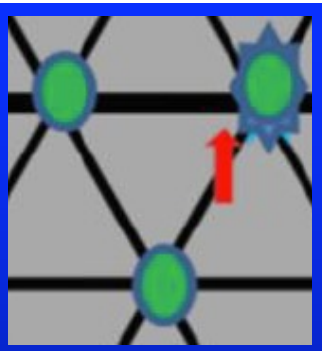

Thank you for your attention!

SIM-NEURO work-group at IBB